Tunable mechanical properties of [Fe(pyrazine)Au(CN)22]–PVDF composite films with spin transitions

Yurii S Bibik, José E Angulo-Cervera, Rostyslav D Lampeka, Il'Ya Gural'Skiy

Tunable mechanical properties of [Fe(pyrazine){Au(CN)$_2$}$_2$]–PVDF composite films with spin transitions

Yurii S. Bibik,[a,b] José E. Angulo-Cervera,[c] Rostyslav D. Lampeka,[a] Il'ya A. Gural'skiy*[a,b]

[a] Department of Chemistry, Taras Shevchenko National University of Kyiv, 64 Volodymyrska St., 01601 Kyiv, Ukraine.

[b] UkrOrgSyntez Ltd., 67 Chervonotkatska St.,02094 Kyiv, Ukraine.

[c] Laboratoire de Chimie de Coordination CNRS & Université de Toulouse (UPS, INP) 205 route de Narbonne, 31077 Toulouse, France.

Corresponding author:

*Il'ya A. Gural'skiy: illia.guralskyi@univ.kiev.ua.

Abstract

Here we describe the elaboration and investigation of composites prepared from the spin-crossover (SCO) complex [Fe(pyrazine){Au(CN)$_2$}$_2$] and poly(vinylidene fluoride) matrix, with different contents of the active phase (10 – 35 wt%). Optical measurements demonstrated that all composites preserve temperature induced hysteretic spin transitions. Tensile mechanical analysis showed a non-linear change of the Young's modulus upon increase of the complex content. Thermomechanical analysis upon a constant strain demonstrated pronouncable alterations of the applied stress in the SCO region. Composites with smaller loads require less stress to attain a given strain in the high-spin state, however for those with high loads the behaviour is more sofisticated. The modelling of stress vs. temperature behaviour revealed that this may be interpreted through a miscellaneous interplay of expansion of both the polymer and the complex, the contribution of both components to the elastic properties of composites, and the effects of SCO on these properties.

KEYWORDS: composites, phase transitions, mechanical properties, optical properties, elastic properties.

1. Introduction

Spin transition compounds occupy an important place in recent development of new materials due to their ability to be switched between two spin states with different physical properties. This switch can be caused by variable external stimuli: temperature or pressure changes, irradiation with light, influence of magnetic field or guest inclusion. Upon the transition an electronic configuration of a central metal ion changes between low-spin (LS) and high-spin (HS). Each of these states possesses its distinct set of optical, magnetic, electrical and mechanical properties, thus leading to many offered diverse applications.[1–4]

Hofmann-type heterometallic coordination polymers[5] form a large family of Fe(II) spin-crossover compounds.[6,7] They are represented by two- or three-dimensional cyanide-bridged bimetallic compounds with N-donor monodentate or bridging organic ligands. Complexes with pyrazines[8–12], pyrimidines[13] and pyridazines[14] are known for diverse spin transitions. The complex $[Fe(pz)\{Au(CN)_2\}_2]$[10] is worthy of attention with its abrupt transition above room temperature, the absence of guest effects and consequently the high reproducibility of transition cycles. Moreover, upon spin state change it undergoes anisotropic deformations expanding along *c* axis (10.6%) and contracting along *b* axis (9.6%).

Production of composites based on spin-crossover (SCO) complexes is a proven way to extend the versatility of materials with switchable electromechanical and magnetic properties.[15–17] Some of the works have been done to develop new bilayer actuators based on SCO complexes and polymers.[18–21] Reversible movement of the actuating machines is reached as a result of thermally, electro- or photo-induced spin transitions. This type of actuators is perspective for the development of micro- and nanoelectromechanical systems (MEMS and NEMS), artificial muscles and devices for switching applications.[22,23]

Various devices, mainly consisting of bilayer structures, have been constructed and investigated for their actuating properties in response to the spin-state change in coordination complexes, notably this actuating performance is directly related to the elastic parameters of active materials.[24–26]

Here we report on a fabrication of composite films based on $[Fe(pz)\{Au(CN)_2\}_2]$ and poly(vinylidene fluoride) (PVDF). As the spin transition of the obtained films can be readily exploited for actuating purposes, their elastic properties were studied. Despite of the many possible parameters that can affect mechanical response of SCO composites, we focus on the basic thermal behaviour of the films and to define the impact of the inclusion of the SCO complex on the elastic properties of the composite.

2. Experimental

2.1 Materials and methods

Potassium dicyanoaurate ($K[Au(CN)_2]$, CAS Number: 78747-50-9), p-toluenesulfonic acid monohydrate ($CH_3C_6H_4SO_3H{\cdot}H_2O$, ACS reagent, ≥98.5%, CAS Number: 6192-52-5), poly(vinylidene fluoride) (PVDF, M_w~534,000, powder) and 2-butanone (C_4H_8O, ACS reagent, ≥99.0%, CAS Number: 78-93-3) were purchased from commercial sources (Sigma Aldrich). Iron powder (Fe) and pyrazine (pz, $C_4H_4N_2$) were provided by UkrOrgSyntez Ltd. All reagents and chemicals were of analytical- or reagent-grade purity and used without any further purification.

2.2 Synthesis

Iron(II) p-toluenesulphonate hexahydrate ($Fe(OTs)_2{\cdot}6H_2O$) and $[Fe(pz)\{Au(CN)_2\}_2]$ complex were synthesized according to the previously reported procedures[10,27].

2.3 Fabrication of polymer composite films

Poly(vinylidene fluoride) was mixed with 2-butanone (MEK) and heated in a water bath at 60°C until the polymer was completely dissolved (Figure 1). This solution was mixed with a mortar grinded powder of $[Fe(pz)\{Au(CN)_2\}_2]$, which was dispersed by stirring. The obtained suspension was then casted on the heated inert surface (Teflon) and the solvent evaporated (experimental conditions are summarized in Table 1). The samples with higher content were prepared at lower temperatures to prevent their bending upon solvent evaporation. The films obtained were annealed in an oven at 115°C for 2 hours to release the residual stress. Films with filler content over 35% appeared to be brittle and unsuitable for further tensile analysis.

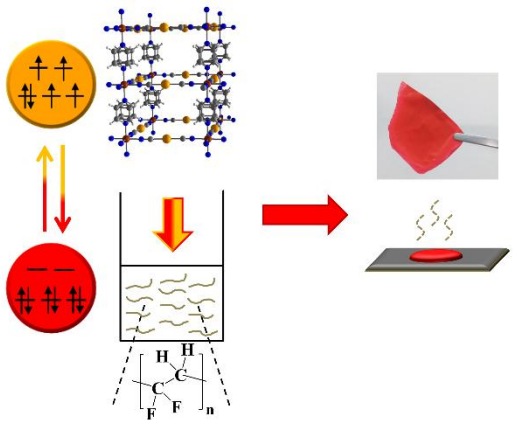

Figure 1. Schematic representation of the of composite films elaboration.

Table 1. The initial combinations of reagents for the film production

wt (%)	m_{SCO} (mg)	m_{PVDF} (mg)	V_{MEK} (ml)	T_{ev} (°C)
10	2	18	0.4	40
15	4.5	25.5	0.4	40
20	5	20	0.4	40
25	5	15	0.5	30
30	6	14	0.5	30
35	8	14.8	0.8	30

2.4 Characterization

2.4.1 Optical measurements

The system for monitoring the spin transition by changing the intensity of the reflected light consisted of an Optica SZM-1 optical microscope equipped with a Sigeta UCMOS 1300 camera. The sample temperature was controlled with a DSC600 Linkam optical cryostat at a heating/cooling rate of 2K/min in a temperature range of 303-403 K. The air was purged off from the stage chamber with dry nitrogen. Photographs were taken automatically using ToupView software (one image per degree). Image processing was performed using ImageJ software.

2.4.2 Mechanical measurements

Tensile properties were studied using a TST350 Linkam cryostat at a heating/cooling rate of 2K/min in a temperature range of 303-403 K. Data processing was performed using Link software. The composite probes where cut in rectangular shape with model parameters (c.a. 20×7.5×0.1 mm).

3. Results and discussion

Composite films were obtained by drop-casting of complex suspensions in PVDF/2-butanone solutions. After further annealing they were studied in temperature-dependent optical and tensile experiments.

3.1 Tensile mechanical analysis

The analysis of the mechanical characteristics of composite films is essential to understand the ability of materials to resist stresses upon different loads. A tensile test involves subjecting of

a composite film to a tension, while a tensile force is followed as a function of elongation. Figure 2 shows a stress vs. strain curve for the 10 wt% composite as a typical mechanical behaviour for a ductile material. The slope of its initial linear part corresponds to Young's modulus of the composite:

$$E = \frac{\sigma}{\varepsilon} \qquad (1)$$

where stress, $\sigma = F/A_0$ and strain, $\varepsilon = \Delta L/L_0$, where F is the tensile force, A_0 is the initial cross-sectional area, L_0 is the initial length and ΔL is the change in length of the specimen[28].

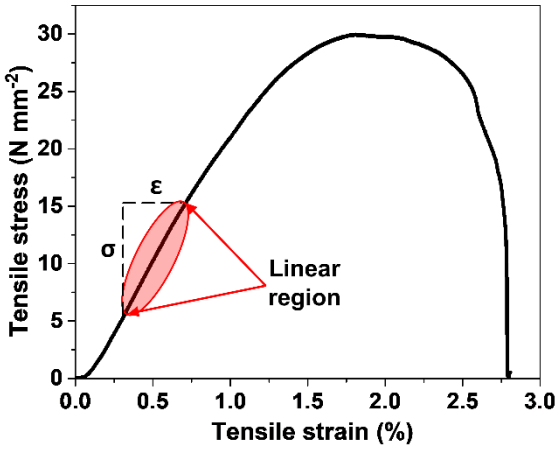

Figure 2. Stress vs. strain curve plotted at 0.1 mm s^{-1} tension indicating the elastic range of deformation for the PVDF composite containing 10 wt% of SCO complex. The slope of the curve can be used to find Young's modulus.

Figure 3 shows Young's modulus of SCO/PVDF composites with different complex load at 303 K. Young's modulus increases with the addition of the SCO complex from 2.0(4) GPa for pure PVDF (this value is in a good agreement with the values found in other works[29,30]) to its maximum value of 2.8(2) GPa at 20 wt%, because the stiffness of the SCO complex is higher compared to PVDF.[31–33] When more filler is added the Young's modulus sharply decreases to 0.51(4) GPa at 35 wt%. This phenomenon is usually caused by interaction between particles and their agglomeration within a matrix. Aggregation turns mechanical behaviour of composites from a ductile to a brittle mode, leading to early failure at the interface and reducing the Young's modulus.[34–36] Juhasz *et al.*[37] showed that smaller particles provide a greater surface area for polymer/filler adhesion resulting in an effective reinforcement of the composite.

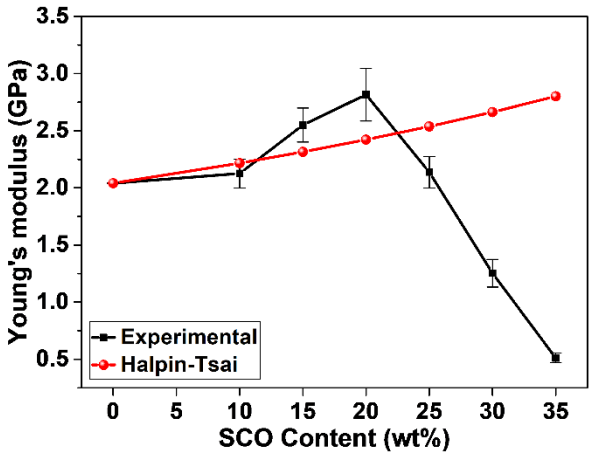

Figure 3. Young's modulus of SCO-PVDF composites as a function of the complex content (experimental data ▪, Halpin-Tsai model ●) at 303 K. Error bars represent standard deviations.

One of the classic models to estimate elastic moduli of polymeric composites comes from Halpin and co-workers.[38] This model was actively used to predict the mechanical reinforcement.[39–43] It describes a modulus of composite as a function of moduli of a polymer and its filler, the shape factor of the particles and the loading direction:

$$E_c = E_{pol}\frac{1+\zeta\eta\varphi_f}{1-\eta\varphi_f} \qquad (2)$$

where E_c and E_{pol} represent the Young's modulus of a composite and a polymer respectively, ζ is a shape parameter dependent on filler geometry and loading direction, φ_f is the volume fraction of the SCO complex, and η is calculated as follows:

$$\eta = \frac{\left(\frac{E_f}{E_{pol}}-1\right)}{\left(\frac{E_f}{E_{pol}}+\zeta\right)} \qquad (3)$$

where E_f represents the Young's modulus of the filler. For the practically isotropic particles used in the present work the aspect ratio is unity, and hence $\zeta = 2$ was used.[44]

Halpin-Tsai approach was applied to model elastic properties of elaborated composites. The Young's modulus of the filler was considered as 7.5 GPa as it was previously obtained for a complex of the similar composition and structure.[18] Volume fractions were calculated from weight fractions and densities of components (1.78 g cm^{-3} for PVDF; 3.13 g cm^{-3} for [Fe(pz){Au(CN)$_2$}$_2$] in LS state[10]):

$$\varphi_f = \frac{w_f\rho_{pol}}{\rho_f(1-w_f)+w_f\rho_{pol}} \qquad (4)$$

where ρ and w are the density and weight fraction, respectively; *pol* refers to PVDF and *f* refers to the SCO complex. Figure 3 compares experimental data with theoretical values obtained from the Halpin-Tsai model for the composites in the LS state. One can see that for <20 wt% composites a predictable growth is observed with some deviation from the Halpin-Tsai model. Some inhomogeneity of composites, anisotropy of particles and their preferential orientation may contribute to this reinforcement.

3.2 Optical detection of spin transitions

SCO is accompanied by a drastic change of the complex colour, that is related to the alteration of *d-d* transitions and MLCT bands upon switching. Obtained films have the colour of the precursor complex: they are intensively red in the LS state and they turn yellow when transit to the HS state. Spin transitions in the polymer/SCO films were studied by following their optical reflectance upon the temperature change. All prepared composites showed an abrupt SCO with a wide thermal hysteresis loop (Figure 4). Temperatures of transition are progressively shifted (Table 1) which can be explained by elastic interactions between the complex and the matrix. Notably, the thermal expansion of the polymer may also affect the transition. One may notice a hysteresis growth for >20 wt% composites which is possibly related to the agglomeration of the SCO particles (this effect was also observed in mechanical measurements). Such agglomeration leads to the interaction between complex particles and increases the cooperativity of the system.

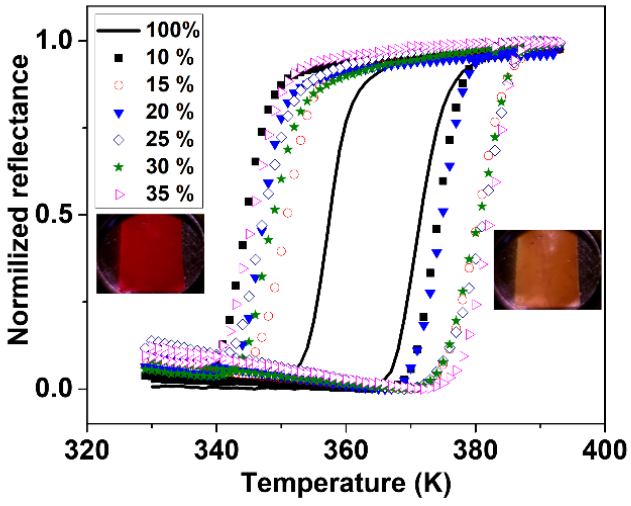

Figure 4. Spin transition related changes in the intensity of reflected light for the complex and its composites. Heating / cooling rates are 2 K min^{-1}. HS and LS photographs of a film (35 wt%) are inserted.

Table 2. Temperatures of the spin transitions for the bulk complex and its composites with PVDF.

wt (%)	100	10	15	20	25	30	35
T_{up} (K)	372	374	380	375	381	380	382
T_{down} (K)	357	345	351	347	347	349	345
ΔT (K)	15	29	29	28	34	31	37

3.3 Thermomechanical detection of spin transition

To follow elastic behaviour of the composites with temperature change, rectangular pieces of a composite films were cut and measured (see Experimental section 2.4.2). Each of these rectangles was studied by fixing it between two clamp holders to be after heated and cooled upon a constant strain, while an effective stress was followed as a function of temperature. The same procedure was repeated at different strains (that did not exceed 1.5% of the initial length of the composite). Far from the spin transition, a gradual decrease of the force necessary to maintain a constant strain was observed upon heating (Figure 5).

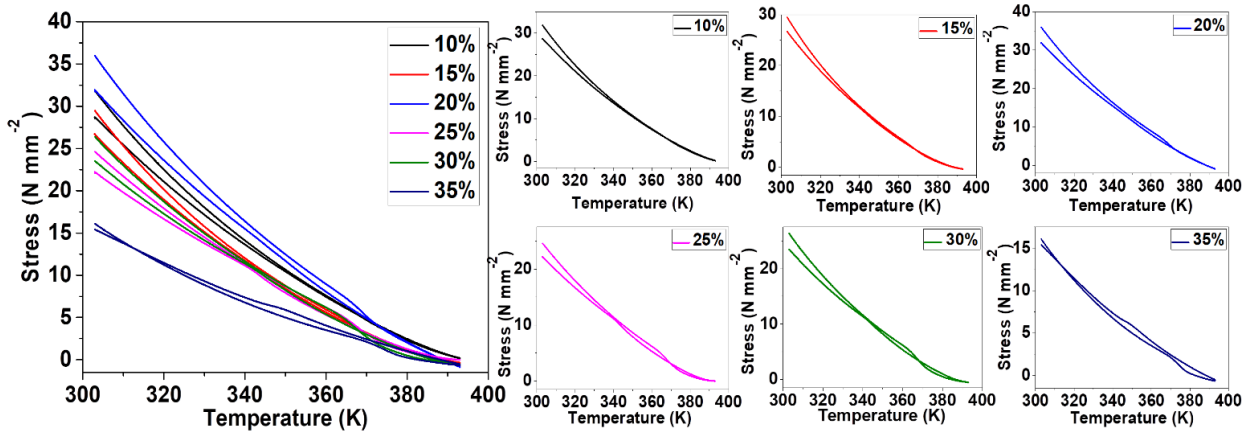

Figure 5. Temperature dependent stress change for PVDF composites with different contents of SCO complex at $\Delta l = 0.175$ mm.

This is primarily caused by the thermal expansion of components (majorly polymer and less complex). Softening of the polymer upon heating also contributes to the "observed stress" drop. However, a pronounceable change in the stress takes place in the SCO region mainly associated with the abrupt expansion/contraction of the complex upon spin transition. This behaviour becomes more evident for composites with higher complex loads (Figure 6a). Also, it is worth to note that at high temperatures and low strain, the measured stress drops to zero because the thermal expansion of the composite reaches (and outreaches) the strain.

The data obtained allowed us to follow directly stress/strain behaviour vs. temperature, however the thermal expansion makes it impossible to extract the Young's moduli of composites at different temperatures (Figure 6c). Nevertheless, a unique thermomechanical behaviour could be spotted through our method: at higher content of the SCO complex (35 wt%) (Figure 6b, d), the HS to LS transition provokes a stress decrease. This may mean that the LS form of the composite is less rigid than the HS, although the complex particles contract.

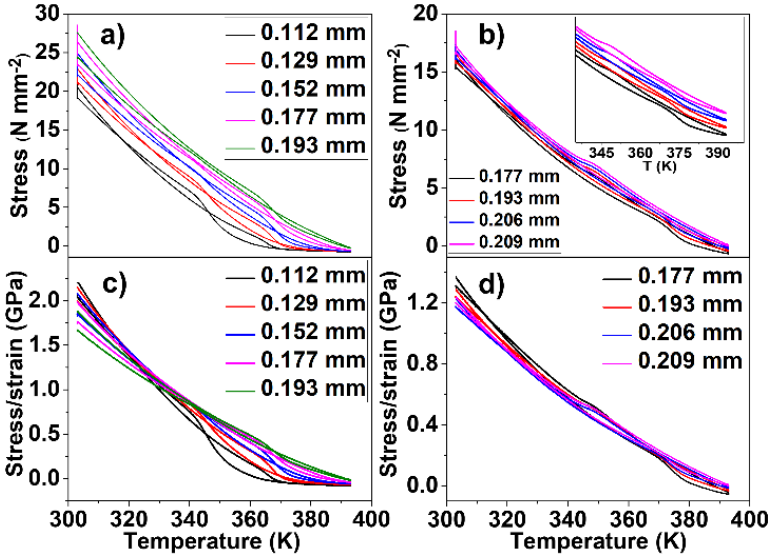

Figure 6. Temperature dependent change of stress at heating / cooling rate of 2 K min-1 for PVDF composite containing 30 wt% (**a**) and 35% (**b**) of SCO complex at different strains. The scaled region of 335-400 K is inserted, the curves are moved apart for easy understanding; Calculated stress/strain ratio vs. temperature for 30 wt% (**c**) and 35 wt% (**d**).

3.4 Elastic properties modelling

Total stress of the polymer composite with the SCO complex in LS state (σ_{LS}) can be derived from the constitutive law of linear thermoelasticity[45]:

$$\sigma_{LS} = E(\varepsilon_0 - \varepsilon_{therm}) = E\left(\frac{\Delta L_0}{L_0} - \alpha_{comp}\Delta T\right) \qquad (5)$$

where ε_0 is an initial strain, ε_{therm} is a strain generated via thermal expansion, ΔT is the temperature above that of ambient, L_0 is an initial length of the specimen and ΔL_0 corresponds to its change upon initial stress application, α_{comp} is a coefficient of linear thermal expansion (CLTE) for a composite. The last can be described as an additive of polymer and complex CLTEs:

$$\alpha_{comp} = \alpha_{pol}\varphi_{pol} + \alpha_{SCO}\varphi_{SCO} \qquad (6)$$

where φ_{pol} and φ_{SCO} stand for volume fractions of the components. Literature data for CLTEs of the polymer and the complex are $\alpha_{pol} = 1.37\times10^{-4}$ K^{-1}, $\alpha_{SCO}^{LS} = 2.80\times10^{-4}$ K^{-1}, $\alpha_{SCO}^{HS} = 1.80\times10^{-4}$ K^{-1}.[10,30] In case of the composite with SCO complex in HS state, eq. (5) should be modified taking into account a strain caused by the spin transition (ε_{SCO}):

$$\sigma_{HS} = E(\varepsilon_0 - \varepsilon_{therm} - \varepsilon_{SCO}) = E\left(\frac{\Delta L}{L_0} - \alpha_{comp}\Delta T - \gamma L_0 \varphi_{SCO}\left(\frac{\Delta V}{V_0}\right)^{1/3}\right) \quad (7)$$

where γ is a coefficient of strain transmission efficiency, $\Delta V/V_0$ is a relative volume change upon SCO.

The temperature dependence of Young's modulus can be assumed as follows[46]:

$$E = E_0 \times exp(-\beta\Delta T) \quad (8)$$

where E_0 is the Young's modulus at the reference temperature (303K), β is a material parameter usually laying in the range between 0.018-0.03 K^{-1} [46–48].

Figure 7 shows calculated stress vs. temperature dependencies for the 30 wt% composite (in both HS and LS states).

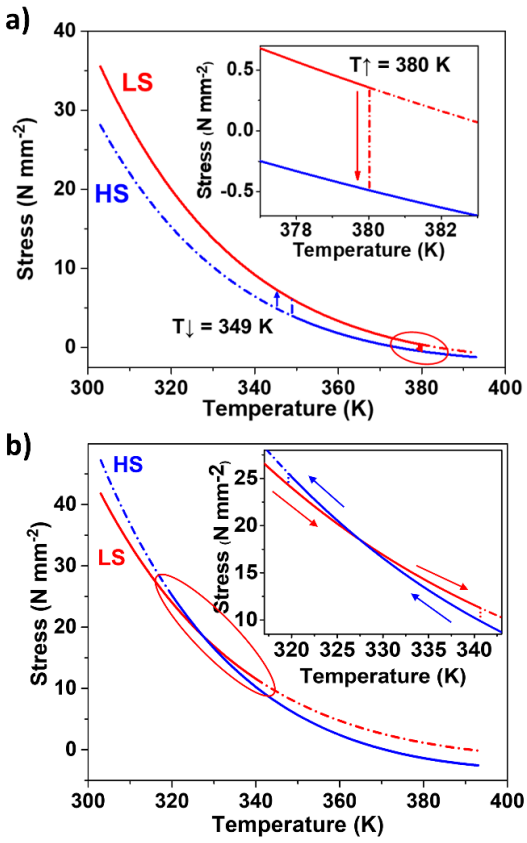

Figure 7. Modelled stress vs. temperature curves for 30 wt% **(a)** and 35 wt% **(b)** $Fe(pz)Au_2(CN)_4$-PVDF composites in LS and HS states at 1.5×10^{-2} initial tensile strain. Magnified selected thermal regions are inserted.

This model can explain the general behaviour of 10-30 wt% filled composites, where the decrease of the stress with temperature is mainly governed by the material parameter (β) and the linear thermal expansion of the composite. The distinction between these curves corresponds to the two spin states and is caused by different volume fractions of complexes (it is higher in HS than LS, while mass fraction stays the same), different linear thermal expansions in different spin states and the strain transmission efficiency. It is possible to model the intersection of the LS and HS curves that is observed for 35 wt% composite (Figure 7b). Also this model considers that Young's modulus and linear expansion coefficients of the complex are higher in HS than in LS state. CLTE for each state is considered as constant within all temperature range, nonetheless, it may fluctuate as was shown by Goodwin et al.[49] for a cyanoheterobimetallic analogue $Ag_3[Co(CN)_6]$. One should also consider that the efficiency of strain transmission tends to decrease with the growth of complex fraction.

While the proposed model is highly empirical, this is the first attempt to interpret tensile properties of spin-crossover composites, and we tried to cover major factors that can affect the behaviour of these polymeric composites.

4. Conclusions

Dispersion of $[Fe(pz)\{Au(CN)_2\}_2]$ in organic polymer PVDF allowed to obtain free standing composite spin-crossover films. Spin-crossover properties of the complex are retained in the composites and can be followed through the change of their optical properties. Tensile mechanical analysis revealed an effect of reinforcement of films that takes place up to 20 wt% load, while higher contents drastically decrease the Young's modulus of the material. Thermomechanical analysis of obtained composites upon constant strain revealed a complicated behaviour for composites of different loads, usually accompanied by a stress drop upon LS to HS transition. However, for the highest load composite, such drop is observed upon both LS to HS and HS to LS transitions, which can be interpreted considering spin state dependent elastic properties of components and their thermal expansion. Obtained results can play an important role in a further development of switchable composite materials and MEMS/NEMS systems. A particular perspective of use for elaborated composites belongs to the electric field effects: piezoelectric PVDF upon external field can affect SCO in the complex and vice versa. This interplay between SCO and piezoelectric properties of composites is of further attention of the authors.

Conflicts of interest

There are no conflicts to declare.

Acknowledgements

This work was supported by Horizon 2020 MSCA-RISE-2016 grant (Project 734322) and Grant 19BF037-01M obtained from the Ministry of Education and Science of Ukraine. JEAC thanks the PhD grant 471690 to CONACyT Mexico. Olesia I. Kucheriv and Volodymyr M. Hiiuk are acknowledged for useful comments on the manuscript.

References

(1) Gütlich, P.; Hauser, A.; Spiering, H. Thermal and Optical Switching of Iron(II) Complexes. *Angew. Chem. Int. Ed. Engl.* **1994**, *33* (20), 2024–2054. https://doi.org/10.1002/anie.199420241.

(2) Molnár, G.; Rat, S.; Salmon, L.; Nicolazzi, W.; Bousseksou, A. Spin Crossover Nanomaterials: From Fundamental Concepts to Devices. *Adv. Mater.* **2018**, *30* (5), 1703862. https://doi.org/10.1002/adma.201703862.

(3) Brooker, S. Spin Crossover with Thermal Hysteresis: Practicalities and Lessons Learnt. *Chem. Soc. Rev.* **2015**, *44* (10), 2880–2892. https://doi.org/10.1039/c4cs00376d.

(4) Otsubo, K.; Haraguchi, T.; Kitagawa, H. Nanoscale Crystalline Architectures of Hofmann-Type Metal–Organic Frameworks. *Coordination Chemistry Reviews*. Elsevier B.V. 2017, pp 123–138. https://doi.org/10.1016/j.ccr.2017.03.022.

(5) Hofmann, K. A.; Höchtlen, F. Abnorme Verbindungen Des Nickels. *Berichte der Dtsch. Chem. Gesellschaft* **1903**, *36* (1), 1149–1151. https://doi.org/10.1002/cber.190303601237.

(6) Muñoz, M. C.; Real, J. A. Thermo-, Piezo-, Photo- and Chemo-Switchable Spin Crossover Iron(II)-Metallocyanate Based Coordination Polymers. *Coord. Chem. Rev.* **2011**, *255* (17–18), 2068–2093. https://doi.org/10.1016/j.ccr.2011.02.004.

(7) Kucheriv, O. I.; Fritsky, I. O.; Gural'skiy, I. A. Spin Crossover in Fe^{II} Cyanometallic Frameworks. *Inorganica Chim. Acta* **2021**, *521*, 120303. https://doi.org/10.1016/j.ica.2021.120303.

(8) Aravena, D.; Castillo, Z. A.; Muñoz, M. C.; Gaspar, A. B.; Yoneda, K.; Ohtani, R.; Mishima, A.; Kitagawa, S.; Ohba, M.; Real, J. A.; Ruiz, E. Guest Modulation of Spin-Crossover Transition Temperature in a Porous Iron(II) Metal-Organic Framework: Experimental and Periodic DFT Studies. *Chem. Eur. J.* **2014**, *20* (40), 12864–12873. https://doi.org/10.1002/chem.201402292.

(9) Kucheriv, O. I.; Shylin, S. I.; Ksenofontov, V.; Dechert, S.; Haukka, M.; Fritsky, I. O.; Gural'skiy, I. A. Spin Crossover in Fe(II)-M(II) Cyanoheterobimetallic Frameworks (M = Ni, Pd, Pt) with 2-Substituted Pyrazines. *Inorg. Chem.* **2016**, *55* (10), 4906–4914. https://doi.org/10.1021/acs.inorgchem.6b00446.

(10) Gural'skiy, I. A.; Golub, B. O.; Shylin, S. I.; Ksenofontov, V.; Shepherd, H. J.; Raithby, P. R.; Tremel, W.; Fritsky, I. O. Cooperative High-Temperature Spin Crossover Accompanied by a Highly Anisotropic Structural Distortion. *Eur. J. Inorg. Chem.* **2016**, *2016* (19), 3191–3195. https://doi.org/10.1002/ejic.201600406.

(11) Gural'skiy, I. A.; Shylin, S. I.; Golub, B. O.; Ksenofontov, V.; Fritsky, I. O.; Tremel, W. High Temperature Spin Crossover in [Fe(Pyrazine){$Ag(CN)_2$}$_2$] and Its Solvate. *New J. Chem.* **2016**, *40* (11), 9012–9016. https://doi.org/10.1039/c6nj01472k.

(12) Levchenko, G.; Gaspar, A. B.; Bukin, G.; Berezhnaya, L.; Real, J. A. Pressure Effect Studies on the Spin Transition of Microporous 3D Polymer [Fe(Pz)$Pt(CN)_4$]. *Inorg. Chem.* **2018**, *57* (14), 8458–8464. https://doi.org/10.1021/acs.inorgchem.8b01124.

(13) Agustí, G.; Gaspar, A. B.; Muñoz, M. C.; Real, J. A. Thermal- and Pressure-Induced Cooperative Spin Transition in the 2D and 3D Coordination Polymers {Fe(5-Br-Pmd)$_z$[$M(CN)_x$]$_y$} (M = Ag^I, Au^I, Ni^{II}, Pd^{II}, Pt^{II}). *Inorg. Chem.* **2007**, *46* (23), 9646–9654. https://doi.org/10.1021/ic700993s.

(14) Gural'skiy, I. A.; Shylin, S. I.; Ksenofontov, V.; Tremel, W. Pyridazine-Supported Polymeric Cyanometallates with Spin Transitions. *Eur. J. Inorg. Chem.* **2019**, *2019* (42), 4532–4537. https://doi.org/10.1002/ejic.201900782.

(15) Chen, Y.; Ma, J. G.; Zhang, J. J.; Shi, W.; Cheng, P.; Liao, D. Z.; Yan, S. P. Spin Crossover-Macromolecule Composite Nano Film Material. *Chem. Commun.* **2010**, *46* (28), 5073–5075. https://doi.org/10.1039/b927191k.

(16) Rat, S.; Nagy, V.; Suleimanov, I.; Molnár, G.; Salmon, L.; Demont, P.; Csóka, L.; Bousseksou, A. Elastic Coupling between Spin-Crossover Particles and Cellulose Fibers. *Chem. Commun.* **2016**, *52* (75), 11267–11269. https://doi.org/10.1039/c6cc06137k.

(17) Piedrahita-Bello, M.; Angulo-Cervera, J. E.; Courson, R.; Molnár, G.; Malaquin, L.; Thibault, C.; Tondu, B.; Salmon, L.; Bousseksou, A. 4D Printing with Spin-Crossover Polymer Composites. *J. Mater. Chem. C* **2020**, *8* (18), 6001–6005. https://doi.org/10.1039/D0TC01532F.

(18) Shepherd, H. J.; Gural'skiy, I. A.; Quintero, C. M.; Tricard, S.; Salmon, L.; Molnár, G.; Bousseksou, A. Molecular Actuators Driven by Cooperative Spin-State Switching. *Nat. Commun.* **2013**, *4* (1), 2607. https://doi.org/10.1038/ncomms3607.

(19) Gural'skiy, I. A.; Quintero, C. M.; Costa, J. S.; Demont, P.; Molnár, G.; Salmon, L.; Shepherd, H. J.; Bousseksou, A. Spin Crossover Composite Materials for Electrothermomechanical Actuators. *J. Mater. Chem. C* **2014**, *2* (16), 2949–2955. https://doi.org/10.1039/c4tc00267a.

(20) Manrique-Juárez, M. D.; Mathieu, F.; Laborde, A.; Rat, S.; Shalabaeva, V.; Demont, P.; Thomas, O.; Salmon, L.; Leichle, T.; Nicu, L.; Molnár, G.; Bousseksou, A. Micromachining-Compatible, Facile Fabrication of Polymer Nanocomposite Spin Crossover Actuators. *Adv. Funct. Mater.* **2018**, *28* (29), 1801970. https://doi.org/10.1002/adfm.201801970.

(21) Manrique-Juarez, M. D.; Mathieu, F.; Shalabaeva, V.; Cacheux, J.; Rat, S.; Nicu, L.; Leïchlé, T.; Salmon, L.; Molnár, G.; Bousseksou, A. A Bistable Microelectromechanical System Actuated by Spin-Crossover Molecules. *Angew. Chem.* **2017**, *129* (28), 8186–8190. https://doi.org/10.1002/ange.201702739.

(22) Rat, S.; Piedrahita-Bello, M.; Salmon, L.; Molnár, G.; Demont, P.; Bousseksou, A. Coupling Mechanical and Electrical Properties in Spin Crossover Polymer Composites. *Adv. Mater.* **2018**, *30* (8), 1–6. https://doi.org/10.1002/adma.201705275.

(23) Manrique-Juarez, M. D.; Rat, S.; Mathieu, F.; Saya, D.; Séguy, I.; Leïchlé, T.; Nicu, L.; Salmon, L.; Molnár, G.; Bousseksou, A. Microelectromechanical Systems Integrating Molecular Spin Crossover Actuators. *Appl. Phys. Lett.* **2016**, *109* (6), 061903. https://doi.org/10.1063/1.4960766.

(24) Mikolasek, M.; Manrique-Juarez, M. D.; Shepherd, H. J.; Ridier, K.; Rat, S.; Shalabaeva, V.; Bas, A. C.; Collings, I. E.; Mathieu, F.; Cacheux, J.; Leichle, T.; Nicu, L.; Nicolazzi, W.; Salmon, L.; Molnár, G.; Bousseksou, A. Complete Set of Elastic Moduli of a Spin-Crossover Solid: Spin-State Dependence and Mechanical Actuation. *J. Am. Chem. Soc.* **2018**, *140* (28), 8970–8979. https://doi.org/10.1021/jacs.8b05347.

(25) Angulo-Cervera, J. E.; Piedrahita-Bello, M.; Mathieu, F.; Leichle, T.; Nicu, L.; Salmon, L.; Molnár, G.; Bousseksou, A. Investigation of the Effect of Spin Crossover on the Static and Dynamic Properties of MEMS Microcantilevers Coated with Nanocomposite Films of $[Fe(Htrz)_2(Trz)](BF_4)$@P(VDF-TrFE). *Magnetochemistry* **2021**, *7* (8), 114.

https://doi.org/10.3390/magnetochemistry7080114.

(26) Dugay, J.; Giménez-Marqués, M.; Venstra, W. J.; Torres-Cavanillas, R.; Sheombarsing, U. N.; Manca, N.; Coronado, E.; Van Der Zant, H. S. J. Sensing of the Molecular Spin in Spin-Crossover Nanoparticles with Micromechanical Resonators. *J. Phys. Chem. C* **2019**, *123* (11), 6778–6786. https://doi.org/10.1021/acs.jpcc.8b10096.

(27) Coucouvanis, D. *Inorganic Syntheses*; Coucouvanis, D., Ed.; Inorganic Syntheses; John Wiley & Sons, Inc.: New York, USA, 2002; Vol. 33. https://doi.org/10.1002/0471224502.

(28) Davis, J. R. *Tensile Testing*; Davis, J. R., Ed.; ASM International: Materials Park, Ohio, USA, 2004. https://doi.org/ttse2004.

(29) Wallner, G. M.; Major, Z.; Maier, G. A.; Lang, R. W. Fracture Analysis of Annealed PVDF Films. *Polym. Test.* **2008**, *27* (3), 392–402. https://doi.org/10.1016/j.polymertesting.2008.01.006.

(30) Xu, Y.; Chung, D. D. L.; Mroz, C. Thermally Conducting Aluminum Nitride Polymer-Matrix Composites. *Compos. Part A Appl. Sci. Manuf.* **2001**, *32* (12), 1749–1757. https://doi.org/10.1016/S1359-835X(01)00023-9.

(31) Zhang, R.; Ying, C.; Gao, H.; Liu, Q.; Fu, X.; Hu, S. Highly Flexible Strain Sensors Based on Polydimethylsiloxane/Carbon Nanotubes (CNTs) Prepared by a Swelling/Permeating Method and Enhanced Sensitivity by CNTs Surface Modification. *Compos. Sci. Technol.* **2019**, *171*, 218–225. https://doi.org/10.1016/j.compscitech.2018.11.034.

(32) Du, Y.; Wu, T.; Yan, N.; Kortschot, M. T.; Farnood, R. Fabrication and Characterization of Fully Biodegradable Natural Fiber-Reinforced Poly(Lactic Acid) Composites. *Compos. B. Eng.* **2014**, *56*, 717–723. https://doi.org/10.1016/j.compositesb.2013.09.012.

(33) Akindoyo, J. O.; Beg, M. D. H.; Ghazali, S.; Heim, H. P.; Feldmann, M. Effects of Surface Modification on Dispersion, Mechanical, Thermal and Dynamic Mechanical Properties of Injection Molded PLA-Hydroxyapatite Composites. *Compos. Part A Appl. Sci. Manuf.* **2017**, *103*, 96–105. https://doi.org/10.1016/j.compositesa.2017.09.013.

(34) Zhang, R.; Hu, H.; Liu, Y.; Tan, J.; Chen, W.; Ying, C.; Liu, Q.; Fu, X.; Hu, S.; Wong, C. P. Homogeneously Dispersed Composites of Hydroxyapatite Nanorods and Poly(Lactic Acid) and Their Mechanical Properties and Crystallization Behavior. *Compos. Part A Appl. Sci. Manuf.* **2020**, *132*, 105841. https://doi.org/10.1016/j.compositesa.2020.105841.

(35) Zhang, X.; Jia, Y. B.; Lu, X. B.; Li, B.; Wang, H.; Sun, L. C. Intramolecularly Two-Centered Cooperation Catalysis for the Synthesis of Cyclic Carbonates from CO_2 and Epoxides. *Tetrahedron Lett.* **2008**, *49* (46), 6589–6592. https://doi.org/10.1016/j.tetlet.2008.09.035.

(36) Kum, C. H.; Cho, Y.; Seo, S. H.; Joung, Y. K.; Ahn, D. J.; Han, D. K. A Poly(Lactide) Stereocomplex Structure with Modified Magnesium Oxide and Its Effects in Enhancing the Mechanical Properties and Suppressing Inflammation. *Small* **2014**, *10* (18), 3783–3794. https://doi.org/10.1002/smll.201302880.

(37) Juhasz, J. A.; Best, S. M.; Brooks, R.; Kawashita, M.; Miyata, N.; Kokubo, T.; Nakamura, T.; Bonfield, W. Mechanical Properties of Glass-Ceramic A-W-Polyethylene Composites: Effect of Filler Content and Particle Size. *Biomaterials* **2004**, *25* (6), 949–955. https://doi.org/10.1016/j.biomaterials.2003.07.005.

(38) Halpin, J. C. Stiffness and Expansion Estimates for Oriented Short Fiber Composites. *J. Compos. Mater.* **1969**, *3* (4), 732–734. https://doi.org/10.1177/002199836900300419.

(39) Rincón-Iglesias, M.; Lizundia, E.; Costa, C. M.; Lanceros-Méndez, S. Tailoring Electrical and Mechanical Properties of All-Natural Polymer Composites for Environmentally Friendlier Electronics. *ACS Appl. Polym. Mater.* **2020**, *2* (4), 1448–1457. https://doi.org/10.1021/acsapm.9b01098.

(40) Alves, M.; Carlstedt, D.; Ohlsson, F.; Asp, L. E.; Pimenta, S. Ultra-Strong and Stiff Randomly-Oriented Discontinuous Composites: Closing the Gap to Quasi-Isotropic Continuous-Fibre Laminates. *Compos. Part A Appl. Sci. Manuf.* **2020**, *132*, 105826. https://doi.org/10.1016/j.compositesa.2020.105826.

(41) Wang, Z.; Singaravelu, A. S. S.; Dai, R.; Nian, Q.; Chawla, N.; Wang, R. Y. Ligand Crosslinking Boosts Thermal Transport in Colloidal Nanocrystal Solids. *Angew. Chem. Int. Ed.* **2020**, *59* (24), 9556–9563. https://doi.org/10.1002/anie.201916760.

(42) Moradi-Dastjerdi, R.; Behdinan, K. Temperature Effect on Free Vibration Response of a Smart Multifunctional Sandwich Plate. *J. Sandw. Struct. Mater.* **2020**, 1–23. https://doi.org/10.1177/1099636220908707.

(43) Fedotov, A. F. Hybrid Model of Homogenization of Engineering Elastic Moduli of Composites Reinforced with Ellipsoid Particles. *Compos. B. Eng.* **2020**, *182*, 107585. https://doi.org/10.1016/j.compositesb.2019.107585.

(44) Halpin, J. C.; Kardos, J. L. The Halpin-Tsai Equations: A Review. *Polym. Eng. Sci.* **1976**, *16* (5), 344–352. https://doi.org/10.1002/pen.760160512.

(45) Le, Q. X.; Torero, J. L.; Dao, V. T. N. Understanding the Effects of Stress on the Coefficient of Thermal Expansion. *Int. J. Eng. Sci.* **2019**, *141*, 83–94. https://doi.org/10.1016/j.ijengsci.2019.05.016.

(46) Arruda, E. M.; Boyce, M. C.; Jayachandran, R. Effects of Strain Rate, Temperature and Thermomechanical Coupling on the Finite Strain Deformation of Glassy Polymers. *Mech. Mater.* **1995**, *19* (2–3), 193–212. https://doi.org/10.1016/0167-6636(94)00034-E.

(47) Johnsen, J.; Grytten, F.; Hopperstad, O. S.; Clausen, A. H. Influence of Strain Rate and Temperature on the Mechanical Behaviour of Rubber-Modified Polypropylene and Cross-Linked Polyethylene. *Mech. Mater.* **2017**, *114*, 40–56. https://doi.org/10.1016/j.mechmat.2017.07.003.

(48) Li, J.; Zhu, Z.; Li, T.; Peng, X.; Jiang, S.; Turng, L. Quantification of the Young's Modulus for Polypropylene: Influence of Initial Crystallinity and Service Temperature. *J. Appl. Polym. Sci.* **2020**, *137* (16), 48581. https://doi.org/10.1002/app.48581.

(49) Goodwin, A. L.; Calleja, M.; Conterio, M. J.; Dove, M. T.; Evans, J. S. O.; Keen, D. A.; Peters, L.; Tucker, M. G. Colossal Positive and Negative Thermal Expansion in the Framework Material $Ag_3[Co(CN)_6]$. *Science* **2008**, *319* (5864), 794–797. https://doi.org/10.1126/science.1151442.